ARTICLE

Polylactide–Poly(dimethylsiloxane)–Polylactide Triblock Copolymers as Multifunctional Materials for Nanolithographic Applications

Marc D. Rodwogin,[†] Charles S. Spanjers,[‡] C. Leighton,[‡] and Marc A. Hillmyer[†,*]

[†]Department of Chemistry and [‡]Department of Chemical Engineering and Material Science, University of Minnesota, Minneapolis, Minnesota 55455-0431

ABSTRACT Highly immiscible block copolymers are attractive materials for applications in nanolithography due to their ability to self-assemble on length scales that are difficult to access by conventional lithography. The incorporation of inorganic domains into such block copolymers provides etch contrast that can potentially reduce processing times and costs in nanolithographic applications. We explored thin films of polylactide–poly(dimethylsiloxane)–polylactide (PLA–PDMS–PLA) triblock copolymers as multifunctional nanolithographic templates. We demonstrate the formation of well-ordered arrays of hexagonally packed PDMS cylinders oriented normal to the substrate, the orthogonal etchability of these cylinders and the PLA matrix, and the formation of etch-resistant domains that can be used as pattern transfer masks.

KEYWORDS: polylactide · poly(dimethylsiloxane) · block polymer · nanolithography

Self-assembly of strongly segregated block copolymers can yield well-defined, compositionally pure domains on the order of 10 nm that are ideally suited for block copolymer lithography.[1,2] The morphology and domain size can be controlled by tuning the molar mass of the constituent blocks. A variety of techniques such as thermal annealing,[3,4] solvent annealing,[5] external field alignment,[6] and substrate modifications[7−10] have all been developed to improve the degree of long-range order in thin films. Highly ordered arrays of lamellar, cylindrical, and spherical microstructures have been used to pattern uniform arrays of lines,[10] rings,[11] dots,[12] and holes.[13]

Since the first example of block copolymer lithography, where Park *et al.* employed polystyrene–poly(butadiene) (PS–PB) and PS–polyisoprene (PI) masks in the fabrication of dot and antidot arrays,[2] a variety of polymeric systems have been employed,[14−17] but none more than PS–poly(methyl methacrylate) (PMMA).[18] Shortly after the Park *et al.* work, Thurn-Albrecht *et al.* used an electric-field-aligned PS–PMMA precursor to grow an array of Cu nanowires.[19] More recently, Kim *et al.* were able to deposit well-ordered arrays of catalytic iron particles using a PS–PMMA mask, which they used to grow dense arrays of carbon nanotubes.[20] In addition to these and other examples of nanowires and nanotubes,[21] PS–PMMA masks have also been used to pattern arrays of dots,[22−26] holes,[27−29] and lines.[30−32] The widespread usage of PS–PMMA stems from the ability to form well-ordered arrays of PMMA domains oriented normal to the substrate and the relative ease with which the PMMA can be selectively etched *via* UV exposure followed by acetic acid washing. However, the PS–PMMA system is not without its drawbacks. The relatively low Flory–Huggins interaction parameter χ between PS and PMMA requires high molecular weights to achieve microphase separation.[33] Additionally, PS is a relatively poor etch mask, susceptible to pattern degradation by organic solvents, elevated temperatures, and even the etching protocols used for pattern transfer. Attempting to overcome these shortfalls, Si- and Fe-containing groups such as poly(dimethylsiloxane) (PDMS),[34] polyhedral oligomeric silsesquioxane (POSS),[35] and poly(ferrocenylsilane) (PFS)[36] have been incorporated into block copolymer masks. These block copolymers can form well-ordered arrays similar to PS–PMMA, but oxidation of the inorganic block using O_2 reactive ion etching (RIE) forms the corresponding oxide, which is highly resistant to further O_2 RIE and retains the pattern of the original polymeric material. This high etch resistance allows for faithful replication of the polymeric pattern into the underlying material, which has been demonstrated in the formation of dots,[37] rings,[11,38] and lines.[34]

*Address correspondence to hillmyer@umn.edu.

Received for review September 9, 2009 and accepted January 15, 2010.

Published online January 29, 2010.
10.1021/nn901190a

© 2010 American Chemical Society

TABLE 1. PLA−PDMS−PLA Block Copolymers

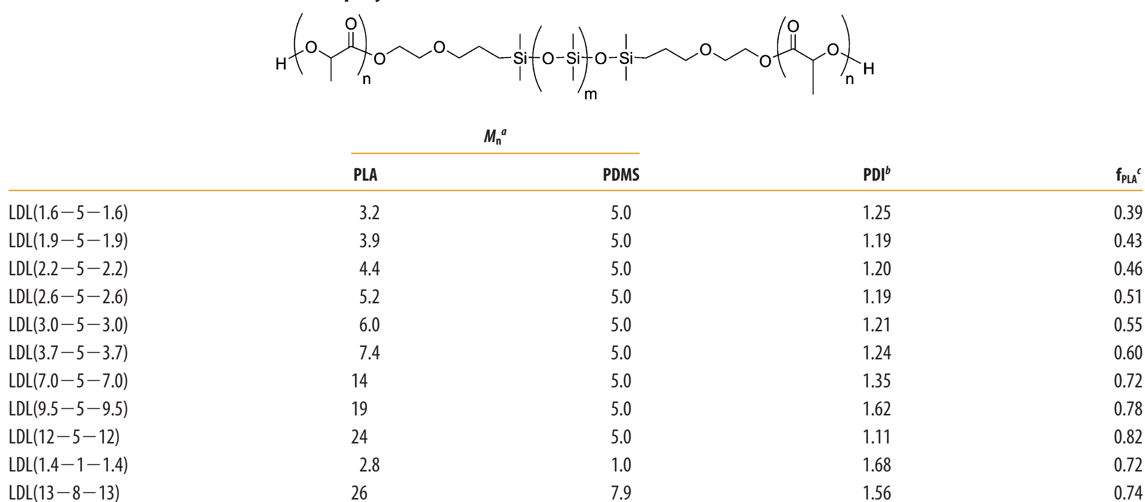

	M_n[a] PLA	M_n[a] PDMS	PDI[b]	f_{PLA}[c]
LDL(1.6−5−1.6)	3.2	5.0	1.25	0.39
LDL(1.9−5−1.9)	3.9	5.0	1.19	0.43
LDL(2.2−5−2.2)	4.4	5.0	1.20	0.46
LDL(2.6−5−2.6)	5.2	5.0	1.19	0.51
LDL(3.0−5−3.0)	6.0	5.0	1.21	0.55
LDL(3.7−5−3.7)	7.4	5.0	1.24	0.60
LDL(7.0−5−7.0)	14	5.0	1.35	0.72
LDL(9.5−5−9.5)	19	5.0	1.62	0.78
LDL(12−5−12)	24	5.0	1.11	0.82
LDL(1.4−1−1.4)	2.8	1.0	1.68	0.72
LDL(13−8−13)	26	7.9	1.56	0.74

[a]Molar masses calculated from ^{1}H NMR spectra assuming two end groups per polymer chain, reported in kg/mol. [b]Polydispersity indices (PDI) were obtained by SEC in chloroform at 35 °C based on PS standards. [c]Volume fractions were calculated at 25 °C from literature densities.[41]

Jung and Ross suggest the ideal block copolymer mask should have a high χ value and possess selectively etchable domains.[34] A large χ value between the constituent blocks favors the formation of well-defined, highly pure domains while the high etch selectivity allows for the pattern formed by these domains to be faithfully transferred into the underlying material. To achieve this goal, we explored the use of an ABA triblock copolymer containing poly(D,L-lactide) (PLA) end blocks and a PDMS midblock. Estimation of χ based on Hildebrand solubility parameters suggests that these two blocks should be extremely incompatible ($\delta_{PLA} = 19.8\ MPa^{1/2}$, $\delta_{PDMS} = 15.1\ MPa^{1/2}$; $\chi_{PDMS-PLA} = 0.94$ at 298 K).[41] The Si in the PDMS backbone provides etch resistance to O_2 RIE, whereas PLA is nearly twice as susceptible to this etchant compared to PS.[39] Conversely, the PDMS domains can be selectively etched in the presence of PLA by fluorinated etchants. This selective etchability provides a route to both dot and antidot arrays. Herein, we will briefly describe the synthesis, molecular characterization, and bulk self-assembly of several PLA−PDMS−PLA block copolymers. We then turn our attention to the thin film behavior of these materials and their use in block copolymer lithography.

RESULTS AND DISCUSSION

We prepared PLA−PDMS−PLA (LDL) triblock copolymers based on established procedures described in the literature.[40,41] Briefly, the ring-opening polymerization of D,L-lactide from a commercially available α,ω-3-(2-hydroxyethoxy)propyl-terminated PDMS (HO−PMDS−OH) macroinitiator was carried out using $Sn(Oct)_2$ at 100 °C either in the bulk or in toluene solution. The LDL samples listed in Table 1 are labeled LDL(X−Y−X), where X is the number average molar mass of each PLA end blocks and Y is the number average molar mass of the PDMS midblock in kg/mol as determined by ^{1}H NMR spectroscopy.

To confirm the formation of PLA−PDMS−PLA triblock copolymers, ^{1}H NMR spectroscopy and size exclusion chromatography (SEC) were employed (see Supporting Information, Figures S1 and S2). Analysis of the ^{1}H NMR spectrum shows a downfield shift of the terminal methylene end groups in HO−PMDS−OH and the emergence of PLA backbone and end group signals. SEC chromatographs of the triblock copolymers show peaks shifted to lower elution volume relative to the parent HO−PDMS−OH homopolymer and PDIs between 1.2 and 1.7. We attribute the variation in PDI to differing levels of PLA homopolymer that appear at roughly the same elution volume as the LDL triblock copolymer and lead to apparent broadening of the SEC traces. The combination of the ^{1}H NMR and SEC results provides strong evidence for the successful initiation of both HO−PDMS−OH hydroxyl groups and the growth of PLA to form PLA−PDMS−PLA triblock copolymers.

Self-assembly of these triblock copolymers in the bulk was probed by small-angle X-ray scattering (SAXS) and transmission electron microscopy (TEM). Every sample examined by SAXS exhibited a primary scattering peak, indicative of microphase separated domains; several samples also exhibit higher order peaks that allow for more precise morphological characterization. Figure 1 shows three representative 1D SAXS profiles consistent with lamellar, cylinder, and sphere forming microstructures. Interestingly, each of these samples retained a relatively narrow principal scattering peak up to 190 °C, indicating that the samples remained microphase separated, despite the high temperatures and relatively low molecular weights. Additionally, we estimated χ using strong segregation theory and the domain spacings of a lamellar sample according to the equation $D = 1.1bN^{2/3}\chi^{1/6}$, where D is the lamellar do-

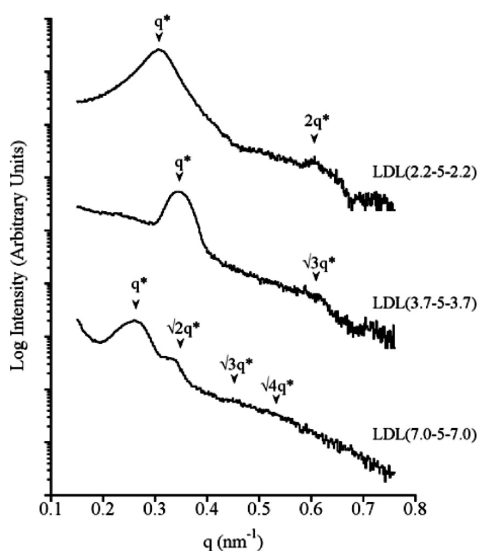

Figure 1. Representative 1D SAXS patterns. Samples consistent with lamellar [LDL(2.2−5−2.2)], cylindrical [LDL(3.7−5−3.7)], and spherical [LDL(7.0−5−7.0)] morphologies are shown. Arrows indicate predicted peak locations for the assigned morphology. Data shown were obtained at 80 °C [LDL(2.2−5−2.2)] or 140 °C [LDL3.7−5−3.7 and LDL(7.0−5−7.0)].

main spacing, b is the statistical segment length, and N is the total degree of polymerization. Using an approximate statistical segment length of 7.9 Å and reference volume of 118 Å^3,[42] $\chi_{PLA-PDMS} = 360/T + 0.21$ was obtained. At 298 K, $\chi \approx 1.4$, in rough agreement with estimates based on solubility parameters. For comparison, at 393 K, we estimate $\chi_{PDMS-PLA} = 1.1$, compared to $\chi_{PS-PMMA} = 0.04$, $\chi_{PS-PLA} = 0.15$, $\chi_{PI-PLA} = 0.24$, and $\chi_{PS-PDMS} = 0.51$.

Figure 2 shows three TEM micrographs of the same lamellar, cylinder, and sphere forming samples shown in Figure 1. The more massive Si atoms in the PDMS domains more efficiently scatter electrons and therefore appear darker. Figure 2 shows block copolymers exhibiting lamellae (Figure 2a), cylinders of PDMS oriented perpendicular to the beam (Figure 2b), and PDMS spheres (Figure 2c). We attribute the disordered nature of the spheres of LDL(7.0−5−7.0) to the extremely large value of χN for this system, which inhibits chain mobility and the ability to adopt structures with long-range order. The domain spacings and feature sizes obtained from these TEM images are consistent with those from SAXS measurements and support the morphological assignments. The presence of two distinct glass transitions around −125 and 40 °C also supports the formation of well-segregated PDMS and PLA domains (Supporting Information Figure S3).

We examined the thin film behavior of the largest block copolymer we prepared, LDL(13−8−13). In the bulk, this block copolymer self-assembles into cylinders of PDMS approximately 28 nm in diameter with a principal domain spacing of 36 nm, as determined by SAXS (see Supporting Information Figure S4). Thin films of LDL(13−8−13) were prepared by spin coating on Au (10 nm)-capped Ni/Cr (3.5 nm) substrates from chlorobenzene or toluene solutions (10 mg mL^{-1}). Solutions in both solvents were macroscopically homogeneous, but images obtained by atomic force microscopy (AFM) showed that films prepared from chlorobenzene were significantly rougher than those prepared from toluene. For that reason, toluene was the preferred spinning solvent.

After spin coating, film thicknesses of approximately 40 nm were measured by imaging a scratched region in the film by AFM as well as by grazing incidence X-ray reflectivity. Height images acquired in tapping mode of the as-spun films showed uniform circular surface features we attribute to a cylindrical morphology consisting of a disordered array of PDMS cylinders oriented normal to the substrate in a PLA matrix (Figure 3a). We attribute the formation of a cylindrical morphology in the case of LDL(13−8−13) as opposed to a spherical morphology observed for LDL(7.0−5−7.0) to the larger degree of segregation of LDL(13−8−13). The apparent observation of a surface perpendicular microstructure is remarkable, considering the large difference in surface energies between PLA and PDMS (approximately 40 and 20 mJ m^{-2}, respectively).[43,44] Large differences in the surface energy of constituent blocks favor

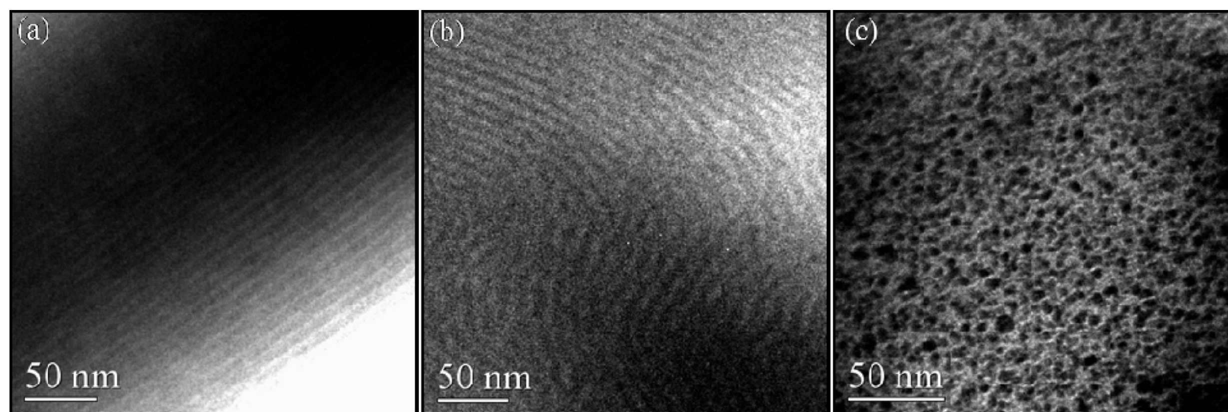

Figure 2. TEM micrographs of (a) LDL(2.2−5−2.2), (b) LDL(3.7−5−3.7), and (c) LDL(7.0−5−7.0) consistent with lamellar, cylindrical, and spherical morphologies, respectively.

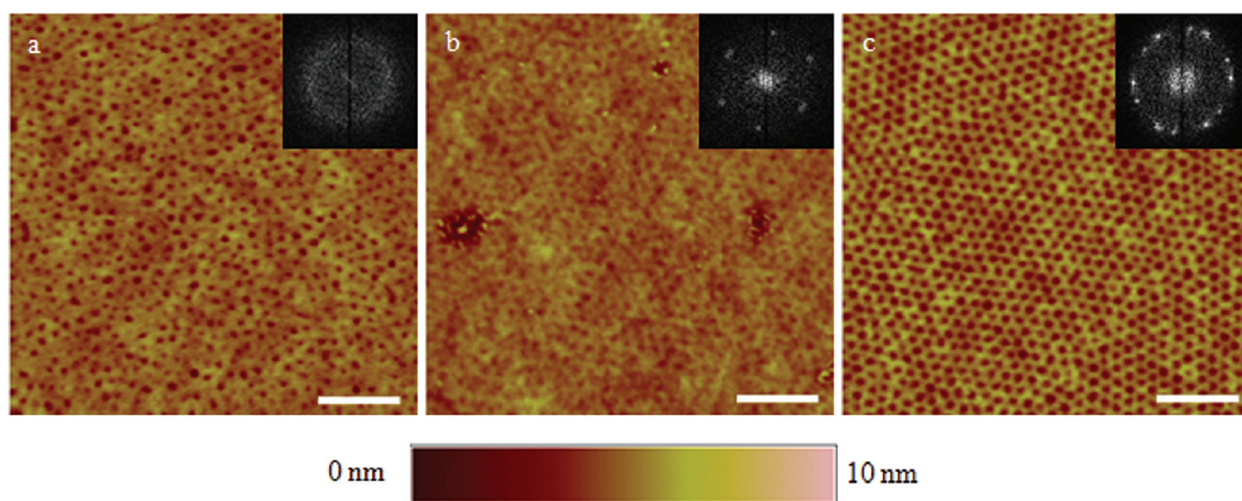

Figure 3. AFM height images of (a) LDL(13−8−13) as spun, (b) after solvent annealing in toluene vapor for 45 min, and (c) after exposure of the solvent-annealed film to 20 s SF_6 RIE. Insets show FFTs obtained from the images. Scale bar 200 nm.

a surface parallel morphology, in an attempt to minimize the exposure of the higher surface energy block to the free surface.[45] To determine if the observed perpendicular morphology was due to incommensurability between the film thickness and domain spacing, films of thickness 20, 70, and 100 nm were also prepared. In each case, uniform circular surface features of identical diameter and pitch indicative of surface normal cylinders were observed. This suggests that the perpendicular orientation of the cylinders is not the result of confinement. This effect may be due to a solvent evaporation gradient normal to the substrate that forms during the spin coating process.[5,46]

To improve the lateral ordering of the system, the films were solvent-annealed under toluene vapor for varying times. After solvent annealing, the contrast of the AFM image was significantly reduced (Figure 3b and Supporting Information Figure S7), suggesting the formation of a thin surface-wetting layer, presumably of PDMS (due to its lower surface energy). As shown in Figure 3c, this wetting layer was removed after 20 s of a SF_6 reactive ion etch (RIE), a PDMS etchant with an approximate etch rate of 80 nm/min.[47] The greatest degree of lateral order was observed after 45 min of toluene vapor exposure. Solvent annealing for less than 45 min or more than 120 min produced films with little long-range order (Figure S6). Interestingly, none of the films displayed islands, holes, or any measurable change in film thickness after solvent annealing up to 480 min. While grain boundaries are clearly observed in the 1×1 μm^2 AFM images, macroscopically uniform films have been reproducibly prepared on 3×3 cm^2 substrates.

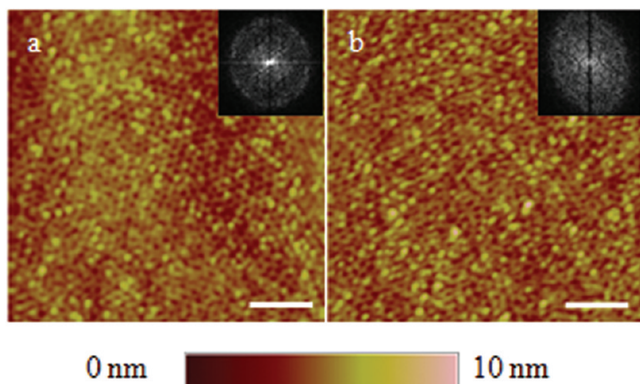

Figure 4. AFM height images after SF_6 RIE for (a) 35 s and (b) 40 s. Films were solvent-annealed for 45 min prior to etching. Insets show the FFT obtained from the images. Scale bar 200 nm.

The ability to selectively etch either the minority cylindrical domains or the majority matrix domain allows for formation of both dot and antidot arrays from the same block copolymer. To probe the etchability of the PDMS domains, solvent-annealed LDL(13−8−13) films were exposed to an additional SF_6 RIE beyond what was needed to remove the surface-wetting layer. Cylindrical features are initially observed after removal of the wetting layer at 20 s of SF_6 RIE (Figure 3c) and are identifiable up to 35 s of SF_6 RIE (Figure 4a), albeit with an apparent decrease in the degree of order. After 40 s of SF_6 RIE, the integrity of the mask starts to become compromised (Figure 4b). This is likely due to the ablation of the mask by high-energy incident ions. To probe the surface of these films, X-ray photoelectron spectroscopy (XPS) was performed (see Supporting Information Figure S5). Prior to SF_6 RIE, the XPS data show signals at binding energies of 531, 284, 151, and 101 eV, corresponding to electrons from the O 1s, C 1s, Si 2s, and Si 2p orbitals, respectively. After 35 s SF_6 RIE, the XPS spectrum showed strong signals at 87 and 82 eV, corresponding to electrons originating from Au $4f^{5/2}$ and $4f^{7/2}$ energy levels. Notably, no signals were observed from either Si 2s or 2p energy levels, consistent with complete removal of the PDMS domains. This agrees well with previously reported high etch rates for Si-containing materials exposed to fluorinated etchants. The results from the XPS data are consistent

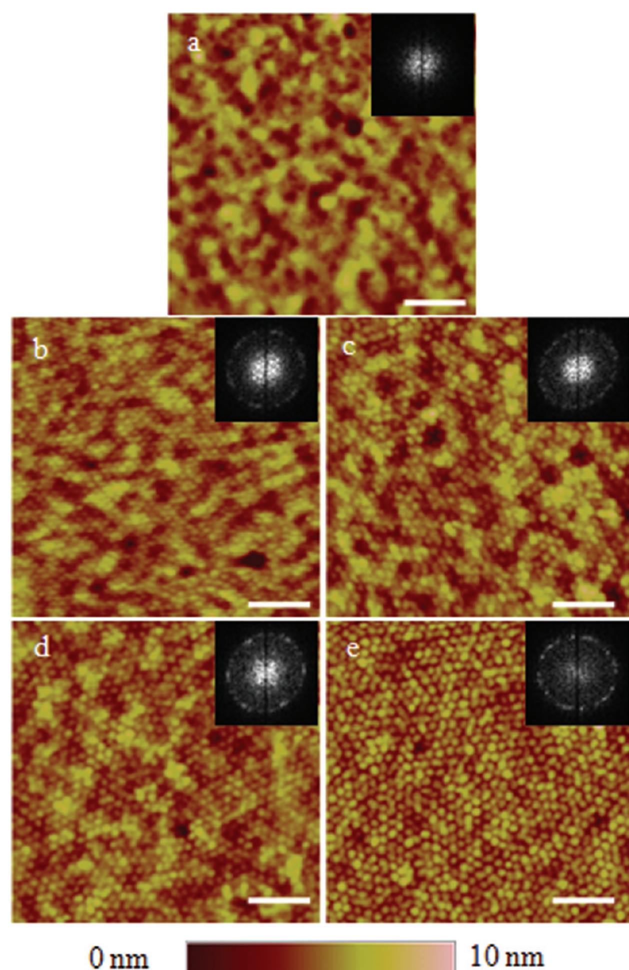

Figure 5. AFM height images after O_2 RIE for (a) 30 s, (b) 60 s, (c) 90 s, (d) 120 s, and (e) 150 s. All films were solvent-annealed for 45 min prior to etching. Scale bar 200 nm.

with ejected Au electrons escaping from cylindrical voids that had previously been occupied by the PDMS domains.

Removal of the PLA matrix and simultaneous oxidation of the PDMS domains to give an array of SiO_x dots were accomplished by exposing solvent-annealed films to an O_2 plasma. Thin film samples were etched in 30 s intervals, and the corresponding AFM images are shown in Figure 5. After 60 s of O_2 RIE, dots were observed. The dots become clearer with increasing exposure to O_2 plasma up to 150 s of RIE, at which point further exposure yields no change in the image. The array of dots exhibits a similar degree of order to the solvent-annealed films, as observed in the FFTs generated from the images. The small interstitial space between the dots and the radius of curvature of the AFM tip prevents accurate measurement of the dot heights. Using an interstitial distance of 13 nm obtained from Figure 3c and the reported tip radius of curvature of 10 nm, we calculate the maximum vertical tip displacement and therefore maximum measurable height to be 2.1 nm. From the AFM images, dot heights of approximately 1.9 nm were measured. After etching, the surface of the film was examined using XPS. In addition to a peak at 284 corresponding to C 1s electrons, the XPS spectrum shows peaks at 151 and 101 eV characteristic of electrons originating from Si 2s and 2p orbitals, respectively, due to the oxidized PDMS. A peak at 531 eV corresponding to O 1s electrons can also be observed, primarily due to the oxidized PDMS, as well. The spectrum also exhibits peaks at 546, 370, and 351 eV, which can be attributed to electrons from the Au $4p^{3/2}$, $4d^{5/2}$, and $4d^{3/2}$ energy levels. Using the relation that 95% of detected electrons originate from a distance less than three times the inelastic mean free path (IMFP) length from the surface[48] and an approximate IMFP length of 1.2 nm[49] for characteristic Au peaks to be observed, any remaining PLA layer is likely less than 3.6 nm thick.

We also attempted to transfer the dot array shown in Figure 5e to the underlying Au layer. To accomplish this, a solvent-annealed and O_2-etched film was subjected to 60 s of Ar ion beam milling. Under similar ion beam milling conditions, etch rates for Au (9.5 nm/min), Ni/Cr (1 nm/min), and SiO_2 (2.5 nm/min) have been previously established.[50] An SEM image after 60 s of Ar ion beam milling shows bright dots of Au on a darker Ni/Cr substrate (Figure 6). From the SEM, the diameter of the dots is approximately 18 nm with a pitch of 27 nm. The cylinder diameter obtained by SEM is slightly smaller than that obtained by AFM (Figure S8), due primarily to distor-

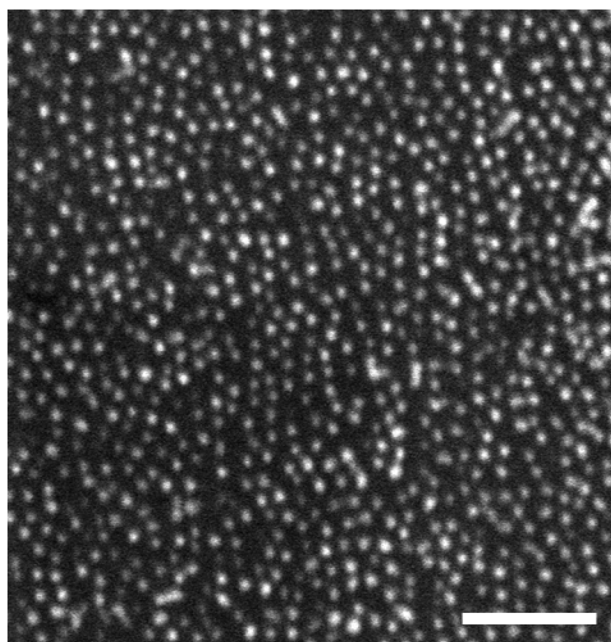

Figure 6. SEM of LDL(13−8−13) after 45 min solvent annealing, 150 s O_2 RIE, and 60 s Ar ion beam milling. Au dots (bright) are observed on a Ni/Cr substrate (dark). Scale bar 200 nm.

ARTICLE

tions caused by the AFM tip. On the basis of the dot size and spacing, we estimate an areal density of 1×10^{12} dot/in^2. Milling for an additional 60 s yielded a disordered array with no easily identifiable pattern. The degradation of the pattern is due to a loss of etch contrast and is a result of the removal of the oxidized PDMS mask. With the mask milled away, the fast-milling Au dots are removed much more quickly than the slow-milling Ni/Cr underlayer, causing the pattern to degrade.

CONCLUSIONS

We employed highly immiscible LDL block copolymer thin films for use in block copolymer lithography. Disordered arrays of cylinders oriented normal to the substrate were obtained directly from spin coating. Solvent annealing under toluene vapor led to the formation of well-ordered hexagonal arrays. Selective etching of the PDMS domains was accomplished using SF_6 RIE and yielded a nanoporous PLA film. Conversely, selective removal of the PLA and oxidation of the PDMS domains was accomplished using O_2 RIE and yielded ordered hexagonal arrays of dots with areal densities on the order of 10^{12} dots/in^2. The utility of these polymers for lithographic applications was demonstrated by transferring the pattern of the oxidized PDMS dots into the underlying Au layer using Ar ion beam milling.

The large value of $\chi_{PDMS-PLA}$ has obvious applications to the continued reduction of lithographically patterned feature sizes. On the basis of our calculated χ parameter, and calculations by Matsen and Thompson,[51] Mayes and Olvera de la Cruz,[52] and Matsen and Schick,[53] we anticipate that a weakly segregated nearly symmetric LDL triblock copolymer (*i.e.*, LDL(0.6−1.0−0.6), $\chi N \approx 20$) with a lamellar microstructure would exhibit PLA and PDMS layers approximately 3.5 nm thick. Features of this size would be among the smallest reported for block copolymers to date.[54] The large value of $\chi_{PLA-PDMS}$, selective etchability, and inherent etch contrast of these materials allow for the fabrication of high density arrays of sub-20 nm domains from small, highly segregated block copolymers. Such high density arrays of small, well-segregated domains may be useful in the fabrication of magnetic recording media or integrated circuits.

EXPERIMENTAL SECTION

Reagents: D,L-Lactide was purchased from Purac and was recrystallized from ethyl acetate and dried *in vacuo* at room temperature prior to use. Stannous octanoate, purchased from Sigma Aldrich, and α,ω-ethoxylpropoxy-terminated poly(dimethylsiloxane), purchased from Gelest, were both used as received. Methylene chloride was purified on an mBraun solvent purification system employing a column of activated alumina. Toluene was purified by passage over activated alumina and supported copper catalysts in a home-built solvent purification system. All other solvents were reagent grade and were used without further purification.

PLA−PDMS−PLA Synthesis: Synthesis of PLA−PDMS−PLA triblock copolymers were carried out in scintillation vials. In one representative polymerization, a vial was charged with 0.8 g (0.18 mmol) of α,ω-ethoxylpropoxy polydimethylsiloxane, 1 g (6.94 mmol) of D,L-lactide, and 0.002 mL of 1 M stannous octanoate (2×10^{-3} mmol). The reaction vessel was then immersed in a 100 °C oil bath for 24 h. After 24 h, the solidified reaction mixture was dissolved in minimal CH_2Cl_2 and precipitated in anhydrous methanol. The recovered product was dried under vacuum for 16 h at room temperature: ^{1}H NMR ($CDCl_3$) δ 5.18 (m, 103 H), 4.33 (m, 1 H), 4.25 (t, J = 5 Hz, 2 H), 3.61 (t, J = 4.5 Hz, 2 H), 3.40 (t, J = 7 Hz, 2 H), 1.58 (m, 2 H), 0.52 (m, 2 H), 0.07 (s, 416 H).

Thin Film Preparation: PLA−PDMS−PLA thin films were prepared from solutions in chlorobenzene or toluene at a concentration of 10 mg mL^{-1} (approximately 0.9% by weight). Polymer solutions were spin coated at 2000 rpm for approximately 30 s onto Si substrates capped with 3.5 nm Ni/Cr and 10 nm Au. Substrates were rinsed in isopropanol prior to spin coating.

Reactive Ion Etching and Ion Milling: O_2 RIE experiments were performed on a Model 320 batch plasma etcher made by Surface Technology Systems. O_2 RIE experiments were done at a process pressure of 1.5×10^{-2} Torr and a chamber power of 20 W. SF_6 RIE experiments were performed on the same instrument with a process pressure and power of 5×10^{-3} Torr and 10 W, respectively. Argon ion beam milling experiments were performed on a Technics argon ion mill using a process pressure of 8×10^{-5} Torr, an acceleration voltage of 100 V, and an ion beam current of 80 mA.

Characterization: ^{1}H NMR spectra were obtained on Varian INOVA-300, INOVA-500, or VXR-300 spectrometers in $CDCl_3$ at room temperature. Samples were prepared by dissolving approximately 25 mg of polymer in approximately 0.750 mL of deuterated chloroform. Each spectrum was obtained after 32 scans with a 25 s pulse delay. Size exclusion chromatography (SEC) was performed on an Agilent 1100 series instrument equipped with an HP 1047A refractive index detector. Three PLgel Mixed C columns as well as a PLgel 5 μm guard column from Varian were employed. Chloroform was used as the mobile phase at 35 °C flowing at a rate of 1 mL/min. Polymer samples were prepared at an approximate concentration of 0.3% (wt/wt) in chloroform. Molecular weights were determined from calibration curves created from narrow molecular weight PS standards purchased from Polymer Laboratories. Differential scanning calorimetry was performed on a TA Instrument Q1000 instrument at a heating rate of 10 °C/min. Nitrogen was used as a purge gas, and instrument calibrations were performed using indium standards. Samples were annealed at 150 °C for 10 min in the instrument before subsequent cooling and heating cycles. Small-angle X-ray scattering was performed at the University of Minnesota Twin Cities Characterization Facility beamline. Cu Kα X-rays (λ = 1.542 Å) were generated by a Rigaku rotating anode equipped with Franks mirror optics. Temperature control was obtained by electrically heating the brass sample holder. Samples at elevated temperatures were annealed for 10 min in the instrument prior to analysis. Two-dimensional SAXS patterns were collected on a Siemens area detector located between 2.2 and 4.4 m from the sample. Prior to morphological characterization, samples were pressed into circular disks approximately 0.5 mm thick at 110 °C in a hydraulic hot press. Transmission electron microscopy images were obtained on a JEOL-JEM 1210 transmission electron microscope operating at an acceleration voltage of 120 kV. Polymer samples were pressed into blocks approximately $20 \times 1 \times 1$ mm^3 at 110 °C and thin sectioned perpendicular to the direction of flow using a Leica EM UC6 Ultramicrotome at room temperature to prepare thin sections for viewing. X-ray photoelectron spectroscopy was performed on an SSX-100 system using a monochromatic Al Kα X-ray source, hemispherical sector analyzer, and a resistive anode detector. Spectra were obtained using an X-ray power of 200 W and a pass energy of 150 eV. Atomic force microscopy was performed on a Digital Instruments NanoscopeII microscope in tapping mode. Engagement set points

between 0.7 and 0.9 of the free amplitude oscillation were used. Scanning electron microscopy was performed on a Hitatchi S900 FE-SEM using an accelerating voltage of 3.0 kV.

Acknowledgment. This work was supported by the MRSEC Program of the National Science Foundation (DMR-0212302 and DMR-0819885) and the National Science Foundation (DMR-0605880). Parts of this work were carried out in the Institute of Technology Characterization Facility and Nanofabrication Center, University of Minnesota, which has received capital equipment funding from the NSF through the MRSEC, ERC, and MRI programs.

Supporting Information Available: ^{1}H NMR spectra and SEC traces of representative LDL block copolymers, as well as XPS spectra after each RIE step and additional SAXS, DSC, and AFM data. This material is available free of charge *via* the Internet at http://pubs.acs.org.

REFERENCES AND NOTES

1. Bates, F. S.; Fredrickson, G. H. Block Copolymers-Designer Soft Materials. *Phys. Today* **1999**, *52*, 32–38.
2. Park, M.; Harrison, C.; Chaikin, P. M.; Register, R. A.; Adamson, D. H. Block Copolymer Lithography: Periodic Arrays of ~1011 Holes in 1 Square Centimeter. *Science* **1997**, *276*, 1401–1404.
3. Hashimoto, T.; Bodycomb, J.; Funaki, Y.; Kimishima, K. The Effect of Temperature Gradient on the Microdomain Orientation of Diblock Copolymers Undergoing an Order-Disorder Transition. *Macromolecules* **1999**, *32*, 952–954.
4. Berry, B. C.; Bosse, A. W.; Douglas, J. F.; Jones, R. L.; Karim, A. Orientational Order in Block Copolymer Films Zone Annealed below the Order−Disorder Transition Temperature. *Nano Lett.* **2007**, *7*, 2789–2794.
5. Kim, S. H.; Misner, M. J.; Xu, T.; Kimura, M.; Russell, T. P. Highly Oriented and Ordered Arrays from Block Copolymers *via* Solvent Evaporation. *Adv. Mater.* **2004**, *16*, 226–231.
6. Morkved, T. L.; Lu, M.; Urbas, A. M.; Ehrichs, E. E.; Jaeger, H. M.; Mansky, P.; Russell, T. P. Local Control of Microdomain Orientation in Diblock Copolymer Thin Films with Electric Fields. *Science* **1996**, *273*, 931–933.
7. Ruiz, R.; Kang, H.; Detcheverry, F. A.; Dobisz, E.; Kercher, D. S.; Albrecht, T. R.; de Pablo, J. J.; Nealey, P. F. Density Multiplication and Improved Lithography by Directed Block Copolymer Assembly. *Science* **2008**, *321*, 936–939.
8. Bita, I.; Yang, J. K. W.; Jung, Y. S.; Ross, C. A.; Thomas, E. L.; Berggren, K. K. Graphoepitaxy of Self-Assembled Block Copolymers on Two-Dimensional Periodic Patterned Templates. *Science* **2008**, *321*, 939–943.
9. Kim, S. O.; Solak, H. H.; Stoykovich, M. P.; Ferrier, N. J.; de Pablo, J.; Nealey, P. F. Epitaxial Self-Assembly of Block Copolymers on Lithographically Defined Nanopatterned Substrates. *Nature* **2003**, *424*, 411–414.
10. Stoykovich, M. P.; Müller, M.; Kim, S. O.; Solak, H. H.; Edwards, E. W.; de Pablo, J. J.; Nealey, P. F. Directed Assembly of Block Copolymer Blends into Nonregular Device-Oriented Structures. *Science* **2005**, *308*, 1442–1446.
11. Jung, Y. S.; Jung, W.; Ross, C. A. Nanofabricated Concentric Ring Structures by Templated Self-Assembly of a Diblock Copolymer. *Nano Lett.* **2008**, *8*, 2975.
12. Olayo-Valles, R.; Lund, M. S.; Leighton, C.; Hillmyer, M. A. Large Area Nanolithographic Templates by Selective Etching of Chemically Stained Block Copolymer Films. *J. Mater. Chem.* **2004**, *14*, 2729–2731.
13. Kubo, T.; Parker, J. S.; Hillmyer, M. A.; Leighton, C. Characterization of Pattern Transfer in the Fabrication of Magnetic Nanostructure Arrays by Block Copolymer Lithography. *Appl. Phys. Lett.* **2007**, *90*, 2333133.
14. Tang, C.; Lennon, E. M.; Fredrickson, G. H.; Kramer, E. J.; Hawker, C. J. Evolution of Block Copolymer Lithography to Highly Ordered Square Arrays. *Science* **2008**, *332*, 429–432.
15. Jung, Y. S.; Jung, W.; Tuller, H. L.; Ross, C. A. Nanowire Conductive Polymer Gas Sensor Patterned Using Self-Assembled Block Copolymer Lithography. *Nano Lett.* **2008**, *8*, 3776–3780.
16. La, Y.-H.; Stoykovich, M. P.; Park, S.-M.; Nealey, P. F. Directed Assembly of Cylinder-Forming Block Copolymers into Patterned Structures to Fabricate Arrays of Spherical Domains and Nanoparticles. *Chem. Mater.* **2007**, *19*, 4538–4544.
17. Zschech, D.; Milenin, A. P.; Scholz, R.; Hillebrand, R.; Sun, Y.; Uhlmann, P.; Stamm, M.; Steinhard, M.; Gösele, U. Transfer of Sub-30-nm Patterns from Templates Based on Supramolecular Assemblies. *Macromolecules* **2007**, *40*, 7752–7754.
18. Ross, C. A.; Cheng, J. Y. Patterned Magnetic Media Made by Self-Assembled Block-Copolymer Lithography. *MRS Bull.* **2008**, *33*, 838–845.
19. Thurn-Albrecht, T.; Schottern, J.; Kästle, G.; Emley, N.; Shibauchi, T.; Krusin-Elbaum, L.; Guarini, K.; Black, C.; Tuominen, M.; Russell, T. Ultrahigh-Density Nanowire Arrays Grown in Self-Assembled Diblock Copolymer Templates. *Science* **2000**, *290*, 2126.
20. Lee, D. H.; Lee, W. J.; Kim, S. O. Vertical Single-Walled Carbon Nanotube Arrays *via* Block Copolymer Lithography. *Chem. Mater.* **2009**, *21*, 1368–1374.
21. Bronikowski, M. J.; Hunt, B. D. Method of Producing Regular Arrays of Carbon Nanoscale Objects Using Nano-Structured Block-Copolymeric Materials for High-Q High-Frequency Nanoscale Oscillators. U.S. Patent Appl. 2003185985; California Institute of Technology, 2003.
22. Kang, G. B.; Kim, S. I.; Kim, Y. H.; Park, M. C.; Kim, Y. T.; Lee, C. W. Tungsten Nanodot Arrays Patterned Using Diblock Copolymer Templates. *Jpn. J. Appl. Phys.* **2007**, *46*, 856–858.
23. McCarthy, W.; Ciszek, P.; Zeghbroeck, B. V.; Borsa, T.; Powers, R. Dial-a-Size: Precision Quantum Dot Nanopatterning Using Cheap, Off-the-Shelf Copolymers. *J. Appl. Polym. Sci.* **2008**, *110*, 3785–3794.
24. Xiao, S.; Yang, X.; Edwards, E. W.; La, Y. H.; Nealey, P. Graphoepitaxy of Cylinder-Forming Block Copolymers for Use as Templates to Pattern Magnetic Metal Dot Arrays. *Nanotechnology* **2005**, *16*, S324–S329.
25. Naito, K. *Chaos* **2005**, *15*, 047507.
26. Kitano, H.; Akasaka, S.; Inoue, T.; Chen, F.; Takenaka, M.; Hasegawa, H.; Yoshida, H.; Nagano, H. Control of the Microdomain Orientation in Block Copolymer Thin Films with Homopolymers for Lithographic Applications. *Langmuir* **2007**, *23*, 6404–6410.
27. Millward, D. B. Two-Dimensional Arrays of Holes with Sub-Lithographic Diameters Formed by Block Copolymer Self-Assembly. U.S. Patent Appl. 2008176767; Micron Technology, Inc., 2008.
28. Asakawa, K.; Hiraoka, T.; Hieda, H.; Sakurai, M.; Kamata, Y.; Naito, K. Nano-Patterning for Patterned Media Using Block-Copolymer. *J. Photopolym. Sci. Technol.* **2002**, *15*, 465–470.
29. Aissou, K.; Kogelschatz, M.; Baron, T.; Gentile, P. Self-Assembled Block Polymer Templates as High Resolution Lithographic Masks. *Surf. Sci.* **2007**, *601*, 2611–2614.
30. Kumar, N.; Hahm, J. Nanoscale Protein Patterning Using Self-Assembled Diblock Copolymers. *Langmuir* **2005**, *21*, 6652–6655.
31. Ruiz, R.; Sandstrom, R. L.; Black, C. T. Induced Orientational Order in Symmetric Diblock Copolymer Thin Films. *Adv. Mater.* **2007**, *19*, 587–591.
32. Stoykovich, M. P.; Kang, H.; Daoulas, K. C.; Liu, G.; Liu, C.; de Pablo, J. J.; Müller, M.; Nealey, P. F. Directed Self-Assembly of Block Copolymers for Nanolithography: Fabrication of Isolated Features and Essential Integrated Circuit Geometries. *ACS Nano* **2007**, *1*, 168–175.
33. Russell, T. P.; Helm Jr., R.; Seeger, P. Temperature Dependence of the Interaction Parameter of Polystyrene and Poly(methyl methacrylate). *Macromolecules* **1990**, *23*, 890–893.

34. Jung, Y.; Ross, C. Orientation-Controlled Self-Assembled Nanolithography Using a Polystyrene−Polydimethylsiloxane Block Copolymer. *Nano Lett.* **2007**, *7*, 2046.
35. Hirai, T.; Leolukman, M.; Liu, C. C.; Han, E.; Kim, Y. J.; Ishida, Y.; Hayakawa, T.; Kakimoto, M.; Nealey, P. F.; Gopalan, P. One-Step Direct-Patterning Template Utilizing Self-Assembly of POSS-Containing Block Copolymers. *Adv. Mater.* **2009**, *21*, 4344–4338.
36. Hempenius, M. A.; Lammertink, R. G. H.; Péter, M.; Vancso, G. J. Poly(ferrocenylsilanes) as Etch Barriers in Nano and Microlithographic Applications. *Macromol. Symp.* **2003**, *196*, 45–56.
37. Ross, C.; Jung, Y.; Chuang, V.; Ilievski, F.; Yang, J.; Bita, I.; Thomas, E.; Smith, H.; Berggren, K.; Vancso, G. Si-Containing Block Copolymers for Self-Assembled Nanolithography. *J. Vac. Sci. Technol., B* **2008**, *26*, 2489–2494.
38. Chuang, V. P.; Ross, C. A.; Gwyther, J.; Manners, I. Self-Assembled Nanoscale Ring Arrays from a Polystyrene-*b*-Polyferrocenylsilane-Poly(2-vinylpyridine) Triblock Terpolymer Thin Film. *Adv. Mater.* **2009**, *21*, 3789–3793.
39. Etch rates were measured on homopolymers films.
40. Kricheldorf, H.; Rost, S.; Wutz, C.; Domb, A. Stereocomplexes of A-B-A Triblock Copolymers Based on Poly(L-Lactide) and Poly(D-Lactide) A Blocks. *Macromolecules* **2005**, *38*, 7018.
41. Zhang, S.; Hou, Z.; Gonsalves, K. E. Copolymer Synthesis of Poly(L-lactide-*b*-DMS-L-lactide) *via* the Ring Opening Polymerization of L-Lactide in the Presence of α,ω-Hydroxylpropyl-Terminated PDMS Macroinitiator. *J. Polym. Sci., Part A: Polym. Chem.* **1996**, *34*, 2737.
42. Ren, Y.; Lodge, T. P.; Hillmyer, M. A. Synthesis, Characterization, and Interaction Strengths of Difluorocarbene-Modified Polystyrene−Polyisoprene Block Copolymers. *Macromolecules* **2000**, *33*, 866–876.
43. Kubo, T.; Wang, R. F.; Olson, D. A.; Rodwogin, M.; Hillmyer, M.; Leighton, C. Spontaneous Alignment of Self-Assembled *ABC* Triblock Terpolymers for Large-Area Nanolithography. *Appl. Phys. Lett.* **2008**, *93*, 133112.
44. Brandrup, J.; Immergut, E.; Grulke, E.; Abe, A.; Block, D., Eds. *Polymer Handbook*, 4th ed.; John Wiley & Sons: New York, 2005.
45. Khanna, V.; Cochran, E.; Hexemer, A.; Stein, G.; Fredrickson, G.; Kramer, E.; Li, X.; Wang, J.; Hahn, S. Effect of Chain Architecture and Surface Energies on the Ordering Behavior of Lamellar and Cylinder Forming Block Copolymers. *Macromolecules* **2006**, *39*, 9346–9356.
46. Temple, K.; Kulbaba, K.; Power-Billard, K. N.; Manners, I.; Leach, K. A.; Xu, T.; Russell, T. P.; Hawker, C. J. Spontaneous Vertical Ordering and Pyrolytic Formation of Nanoscopic Ceramic Patterns from Poly(styrene-*b*-ferrocenylsilane). *Adv. Mater.* **2003**, *15*, 297–300.
47. Min, J. H.; Lee, G. R.; Lee, J. K.; Moon, S. H. Dependence of Bottom and Sidewall Etch Rates on Bias Voltage and Source Power During the Etching of Poly-Si and Fluorocarbon Polymer Using SF_6, C_4F_8, and O_2 Plasmas. *J. Vac. Sci. Technol., B* **2004**, *22*, 893–901.
48. The probability that an electron from depth z is detected is described by $P(z) = e^{(-z/\lambda)}$, where λ is the inelastic mean free path. Substitution of $z = 3\lambda$ yields the conclusion that 95% of detected electrons originate from depths less than 3λ from the surface.
49. Seah, M. P.; Dench, W. A. Quantitative Electron Spectroscopy of Surfaces: A Standard Data Base for Electron Inelastic Mean Free Paths in Solids. *Surf. Interface Anal.* **1979**, *1*, 2–11.
50. Etch rates were established by the Nanofabrication Center, University of Minnesota Institute of Technology.
51. Matsen, M. W.; Thompson, R. B. Equilibrium Behavior of Symmetric ABA Triblock Copolymer Melts. *J. Chem. Phys.* **1999**, *111*, 7139–7146.
52. Mayes, A.; Olvera de la Cruz, M. Microphase Separation in Multiblock Copolymer Melts. *J. Chem. Phys.* **1989**, *91*, 7228–7235.
53. Matsen, M.; Schick, M. Lamellar Phase of a Symmetric Triblock Copolymer. *Macromolecules* **1994**, *27*, 187–192.
54. Park, S.; Lee, D. H.; Xu, J.; Kim, B.; Hong, S. W.; Jeong, U.; Xu, T.; Russell, T. P. Macroscopic 10-Terabit-per-Square-Inch Arrays from Block Copolymers with Lateral Order. *Science* **2009**, *323*, 1030–1033.